Ternary diagrams as a tool for developing ceramic materials from waste. Relationship between technological properties and microstructure

R.J. Galán-Arboledas[1], M.T. Cotes-Palomino[2], C. Martínez-García[2], Moreno-Maroto, J.M[1], Uceda-Rodríguez, M.[1]., S. Bueno[1, 2]

[1] Fundación Innovarcilla. Pol. Ind. El Cruce. C/ Los Alamillos, 25. 23710. Bailén (Jaén). Spain

[2] Department of Chemical, Environmental and Materials Engineering. Technological Scientific Campus of Linares. University of Jaén, Linares, Jaén, 23700, Spain

tecnico@innovarcilla.es, corresponding author

Abstract

In this paper it is proposed the manufacture of ceramic construction materials using only industrial waste from different production processes as raw materials. The selected wastes are electric arc furnace stainless steel slags, EAF-SS, fly and bottom ash from coal power plants, FCA and BCA, and diatomaceous earths from filtration of vegetable oils, DO. From them, the ternary equilibrium diagram SiO_2-Al_2O_3-CaO has been used as a tool for formulating two waste mixtures with a chemical composition in the range of that of clay-based construction materials manufactured by the ceramic industry in Bailén (Jaén, Southern Spain). Additionally, according to their mineralogical composition, these two waste-based materials were formulated in order to get different sintering and technological behavior. One of them, material C, develops refractory crystalline calcium phases, and the other, material D, was formulated in order to display a greater melting capacity.

A microstructural characterization using SEM-EDX was carried out on the sintered materials C and D at three firing temperatures (1000 ºC, 1050 ºC y 1100 ºC) to verify the development of crystalline phases and the evolution of the porosity during the thermal treatment. In addition, the mineralogical composition of the fired specimens has been quantified using the Rietveld methodology and the pore size and distribution has been determined using Mercury Intrusion Porosimetry and Helium Pycnometry.

The determined technological properties were apparent density, water absorption capacity, bending strength and thermal conductivity. This characterization has made it possible to explain the technological properties of the ceramic waste-based compositions according to their formulation and developed microstructure. Obtained results display the suitability of the ternary SiO_2-Al_2O_3-CaO diagram for the design of ceramic compositions from industrial waste.

Keywords: Waste, ceramic materials, ternary phase diagram, technological properties, microstructure.

1. Introduction

Currently, the way to measure the environmental impact and the carbon footprint associated with a product, process or service can be done in different ways, but the Ecodesign and Life Cycle Analysis, LCA, are the most widely used methodologies. These are endorsed in an international regulatory framework, conforming the base for obtaining environmental certifications as the Environmental Product Declarations, EPD, that establishes the European Regulation on Construction Materials (EU) Nº 305/2011 UE.

Eco-design considers functionality, safety, ergonomics and environment when designing a product or service with the aim of reducing the environmental impact that may be produced throughout the life cycle of the product, evaluating suppliers, manufacturers, users and waste managers, according to ISO 14006 standard [1]. In this sense, the so-called "strategies" or "principles" of eco-design have been developed, which encompass the development of new concepts, selection of materials with less impact, reduction of the use of natural resources and of the environmental impact during production and the use stage, promotion of environmentally friendly packaging and logistics, increase in the durability of the product and optimization of the end-of-life system. The first three ones have been taken into account for the development of this work. First, it is intended to develop a new ceramic material made from waste solely, which reduces its associated environmental impact by introducing it into a new life cycle and reduces the consumption of natural resources by not using mineral raw materials in its composition.

In this context, waste recovery should be understood as any operation whose main goal is the transformation of the residue in a potential asset, both for a material and/or energy use, as the European strategy for the efficient use of resources establishes [2]. Many researchers have focused their research on the recovery of industrial waste in ceramic materials due to the suitability of the firing process to release the calorific power of organic residues or to effectively incorporate inorganic waste in the ceramic materials structure [3-6]. The formulation of conventional ceramics produced from natural raw materials (mainly clay) has been successfully performed from tools as the thermodynamic phase equilibrium diagrams or empirical and technological diagrams [7-9]. However, no or little experience is still available in the case of alternative ceramic materials formulated mostly from waste.

Among the inorganic wastes considered, the use of steel mill slag has been proposed by El-Mahllawy [10], together with the use of kaolin and granite quarry waste to produce bricks resistant to chemical actions, particularly wastewater, which improve the properties of conventional materials. Galán-Arboledas et al. [11] studied how the addition of steel slag influences the manufacturing process of ceramic construction materials, analyzing the modification of the energy required for their production, both in the drying and firing process, the environmental impact and how the technological properties of the materials manufactured may be affected. Other references considering the recovery of steel mill ashes have allowed the use of this waste to be validated for the manufacture of a wide range of ceramic products with different degrees of porosity or vitrification [12-20].

Another large family of wastes covered by the scientific literature on development of ceramic materials is coal-fired power plant ash. Thus, Chen et al. [21] studied the addition of hematite residues and fly ash to a clay mixture for brickmaking, while Lingling et al. [22] investigated the production of refractory materials from fired clay by replacing high proportions of clay with fly ash. Romero and Rincón [23] studied the possibility of using different kinds of inorganic waste (from zinc hydrometallurgy, ash from thermal power plants, slag and ash from incineration plants) either individually or by mixing them with other raw materials to obtain materials with wide applications in construction and civil works, concluding that the ceramic and vitroceramic process is a real and useful alternative to solve, at least partially, the social and environmental problems associated with the production of such waste. Further research into the recovery of waste from coal-fired power stations has shown the suitability of this waste for the manufacture of ceramic materials [24-33].

On the other hand, the wastes that incorporate an organic fraction or biomass allow not ony the valorization of the material, but also the recovery of energy, which can also be a valuable alternative in the ceramic industry. That is why Monteiro and Vieira [34] investigated the effect of the addition of an oily residue obtained from an oil separation process on the properties of clay-based ceramics. The results showed that the addition of 5 to 10 wt% of oily residues produces an increase in mechanical strength, while the apparent density, linear shrinkage and water absorption remain unchanged virtually. In general, the filtering earths used in the food and agriculture industry, based on diatomites or zeolites, represent an alternative of interest for the ceramic industry due to their potentially high organic content obtained after the filtration processes [35-41].

Therefore, it can be remarked that the use in the construction sector of ceramic products manufactured from wastes is an option that fits perfectly with the principles of sustainable development, since it represents a valuable solution that allows the reuse of materials that are currently considered as useless. In addition, many studies demonstrate that the addition of wastes may involve significant enhancements in the ceramic material properties, apart from contributing to a better management from an environmental perspective. For this reason, the present paper aims to manufacture ceramic materials for construction from different selected wastes: electric arc furnace steel slag, coal-fired power plant ash and oil-filtering diatomaceous earth, for which the ternary phase equilibrium SiO_2-Al_2O_3-CaO diagram will be employed as a tool for designing the materials formulations.

2. Materials and Methods

2.1. Raw Materials

Only industrial wastes (supplied by waste manager FCC-Ambito, Spain) have been used as raw material to perform the present study. On the one hand, wastes of an inorganic nature have been employed: steel ashes (EAF-SS), coal bottom ashes (BCA), carbon fly ashes (FCA), which are residues generated in the manufacturing of stainless steel and during the combustion of coal in thermal-power plants, respectively. On the other hand, a mixed-nature waste has also been studied, oil-filtering diatomaceous-earth (DO), which is made up of inorganic and organic components. This waste has its origin in the vegetable-oil purification industries when using diatomaceous earth as filter media.

The four residues used as raw material have been subjected to a series of characterization tests, which have been focused on the determination of the chemical and mineralogical composition (Table 1) along with simultaneous thermal analysis to understand their behavior when undergoing a thermal cycle. The results obtained from this characterization are found in [15]. A reference clay-based material, used by the ceramic industry in Bailén (Jaén, Southern Spain) to manufacture structural ceramics, has been coded as R and is described in [42].

Table 1: Chemical and mineralogical composition of clay-based reference material (R) and waste selected as raw materials

	SiO_2	Al_2O_3	Fe_2O_3	MgO	CaO	Na_2O	K_2O	MnO	TiO_2	P_2O_5	Cr_2O_3	SO_3	LOI
EAF-SS	33,0	9,7	0,9	7,2	39,8	0,1	0,4	1,4	1,1	0,1	2.8	0.3	2.6
BCA	47,3	23,2	8,4	2,3	3,8	1,2	1,8	0,1	1,3	1,1	-	2.6	5.7
FCA	50,8	22,8	11,5	1,2	2,7	1,1	2,3	0,1	1,1	0,3	-	1.3	4.7
DO	36,1	2,4	0,9	16,2	3,1	0,1	0,6	0,1	0,1	0,2	-	0.1	40.0
R	54.2	12.4	4.6	2.2	9.7	1.0	3.2	0.1	0.5	0.1	-	0.7	11.9

*LOI: Loss on ignition

	Q	M	H	A	Me	C	D	B	Phy	A/V
EAF-SS	10	-	-	25	35	10	-	-	-	20
BCA	17	17	5	-	-	-	-	5	-	55
FCA	25	15	10	-	-	-	-	-	-	50
DO	5	-	-	-	-	5-10	-	-	-	*
R	37	-	-	-	-	15	6	-	42	-

Q: Quartz; M: Mullite; H: Hematite; A: Akermanite; Me; Merwinite; C: Calcite; D: Dolomie; B: Basanita; Phy: Phyllosilicates and A/V: Amorphous/Vitreous and Tr: Traces (1-3 %).

* It has not been possible to quantify the amount of amorphous phase. although there is a substantial amount

2.2. Materials Formulation

The phase equilibrium ternary diagram SiO_2-Al_2O_3-CaO [7] has been used with the objective of formulating materials whose chemical composition is located in the same area as the traditional clay-based ceramic material, R, namely in the anortite (CAS_2) primary field, as shown in Figure 1.

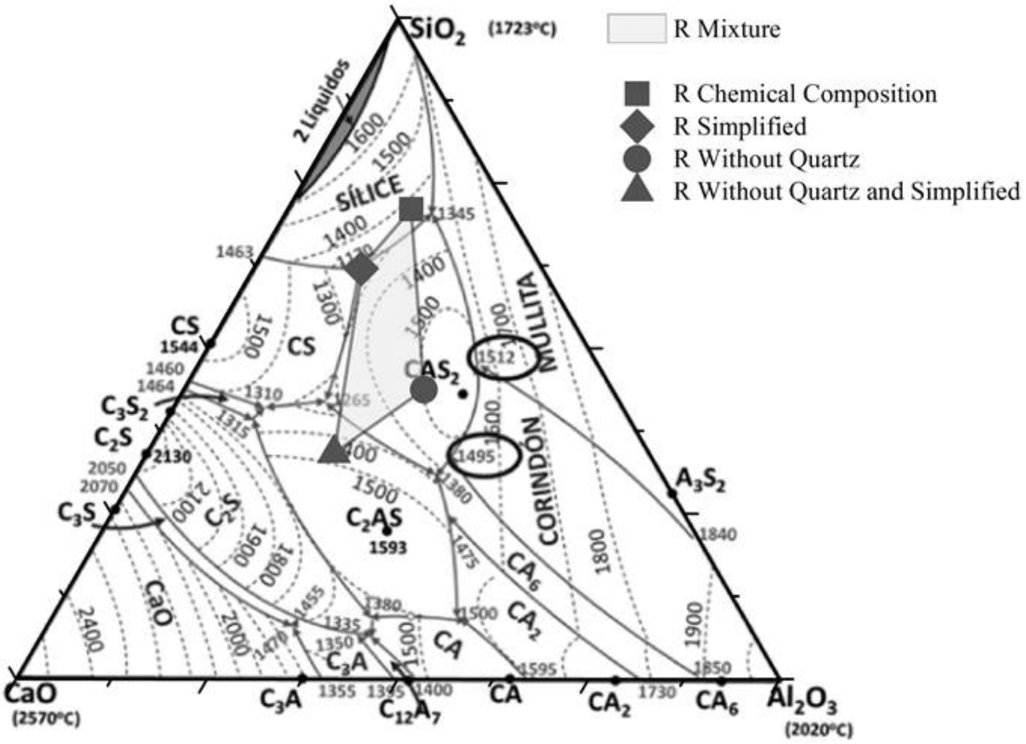

Figure 1: Reference region in the SiO_2-Al_2O_3-CaO diagram for the formulation of waste based compositions

Phase equilibrium diagrams display stable phases according to thermodynamic of pure reactive components in the system. However, actual stability of phases depends on raw materials reactiveness, reaction kinetic and the presence of minor components or impurities modifying the course of transformation reactions during the thermal treatment. From this fact, and in order to consider a wider area for formulating the materials, a series of chemical compositions defining the vertices of a formulation region have been calculated (Fig. 1). The different chemical compositions are defined below:

- Chemical composition: It is defined as the percentage by weight of the proportions of SiO_2, Al_2O_3 and CaO quantified in the chemical composition and recalculated to 100%.
- Reactive Chemical Composition without Quartz: It is defined as the percentage by weight of the previous proportions, restated to 100%, but in which the chemical quantification of SiO_2 has been corrected by subtracting the quartz percentage from the mineralogical composition

in Table 1 (in ceramic materials quartz remains inert, without reacting, until approximately 1100 ºC).

- Simplified Chemical Composition: It is defined as the percentage by weight of the proportions of SiO_2, Al_2O_3 and CaO quantified in the chemical composition (and corrected to 100%) but also associating these components with the minor compounds according to their physicochemical characteristics. Thus, glass-forming compounds (MgO, K_2O and Na_2O) have been associated with CaO. Also Fe_2O_3 has been related to CaO, since Fe replaces Ca in the compounds formed in this system. Minor components have not been considered as well as those that are in equivalent proportions in all materials (TiO_2, P_2O_5 and MnO).
- Simplified Reactive Chemical Composition without Quartz: It is defined as the combination of the above mentioned compositions without reactive quartz and the simplified one.

Besides presenting a chemical composition similar to that of traditional ceramic materials, it is intended to obtain two different technological behaviours. On the one hand, a porous refractory material in which calcium crystalline phases have been developed, and on the other hand, a porous material but with a greater melting capacity. Therefore, the specific criteria followed to formulate each waste mixture are detailed below:

- Material C: It contains Ca-bearing waste such as steel slag, EEA-SS, and coal bottom ash, BCA. It is expected that calcium crystalline phases are developed, thus this material yield a high porosity, with an acceptable mechanical strength. [43]
- Material D: Apart from coal fly ash, FCA, its formulation includes the oil diatomaceous-earth, DO, with a significant amount of amorphous silica promoting melting capacity and a more vitreous microstructure [40]. Consequently, this material display lower porosity than material C and a higher mechanical strength.

2.3. Processing and Characterization Methods

The waste-mixtures were shaped by pressing as described in [15] and then the resulting pieces were sintered in an electric chamber kiln (CBN-50, Kittec CB, Germany) for 3 hours at the maximum temperature, in this case 1000 ºC, 1050 ºC and 1100 ºC. On the fired specimens, microstructural characterization was carried out to determine the porosity and the mineralogical phases formed during the thermal treatment. Likewise, the main technological properties were determined in order to know if the final characteristics obtained correspond to the formulation expectations and make these materials technically viable.

The microstructural characterization consisted in determining the microstructure developed by the materials at different sintering temperatures by combining the mercury intrusion porosimetry technique (Autopore IV 9500, Micromeritics, USA) to determine the pore size distribution in the 0.005-360 μm equivalent diameter range, with observations by SEM-EDX microscopy (JSM-6010 LA, Jeol, Japan) to assess the shape, size and distribution of pores and phases throughout the sample.

For the identification and quantification of the crystalline phases developed in the sintered materials, the quantitative mineralogical analysis was carried out on a PANalytical XPert PRO MPD diffractometer (Holland) with CuKα1 radiation. The tube worked at 45 kV and 40 mA and the measurements were made from 5º to 70º (2θ) for 2 h. Rietveld refinement method was used to quantify the contribution (% by weight) of each crystalline phase by means of the software PANalytical High Score Plus (HSP). Furthermore, in order to study the percentage of amorphous material, a second diffractogram of each material was obtained by mixing the samples with an alumina standard and performing the test under similar conditions but for a longer time (5 h).

Regarding the technological properties, the main parameters that have been determined were the bulk density, relying on the Archimedes principle, the water absorption capacity according to the UNE-EN ISO 10545-3 standard and the 3 point bending strength (CM-C, Hoytom, Spain) carried out with 60 mm span and a displacement rate of 5 mm/min. In addition, the thermal conductivity of the materials was determined by an adaptation of the hot-wire technique (THB-1, Linseis, Germany), based on the EN 993-15 standard. Finally, the determination of absolute density was conducted by helium pycnometry (AccuPyc II 1340, Micromeritics, USA). Reported results for the apparent density and water absorption tests corresponded to the average value of three determinations, while six determinations were considered in the case of the flexural strength and the thermal conductivity. The standard deviation was assumed as the error of the measurements.

3. Results and Discussion

3.1. Formulation of Mixtures

Based upon the chemical composition of the wastes used as raw materials and with the final objective of obtaining waste-based amterials that present a chemical composition similar to that of R, reference ceramic construction material, Materials C and D have been formulated in order to be located within the primary field of anortite (CAS2) in the ternary diagram of phase equilibrium SiO_2-Al_2O_3-CaO [7], as described in Section 2.2. Hence, for material C it is proposed a mixing formulation formed by 35 wt% of EAF- SS, and 65 wt% of BCA, while the material D is made up of 80 wt% of FCA plus 20 wt% of DO. Table 2 shows the chemical composition of the waste-based materials C and D, together with the chemical composition of the reference material R.

Table 2: Chemical composition of formulated materials (C and D) and reference clay material (R)

	SiO_2	Al_2O_3	Fe_2O_3	MgO	CaO	Na_2O	K_2O	MnO	TiO_2	P_2O_5	Cr_2O_3	SO_3	LOI
C	42.3	18.5	5.8	4.0	16.4	0.8	1.3	0.6	1.2	0.8	1.0	1.8	4.6
D	47.9	18.7	9.4	4.2	2.8	0.9	2.0	0.1	0.9	0.3	-	1.1	11.8

*LOI: Loss on ignition

Once the chemical composition of materials C and D has been determined, the simplified chemical composition, the quartz-free reactive chemical composition and the quartz-free simplified reactive chemical composition are calculated so that they can be represented in the ternary phase equilibrium diagram SiO2-Al2O3-CaO, thus obtaining the formulation region for obtaining the desired materials. Table 3 shows the different chemical compositions used to obtain the region of formulation within the SiO_2-Al_2O_3-CaO ternary phase equilibrium diagram, which are depicted in Figure 2.

Table 3: SiO_2, Al_2O_3 and CaO (wt. %) corresponding to the points forming the formulation region of C and D materials in the ternary diagram. R compositions are also included.

	C Mixture			D Mixture			R Mixture		
	SiO_2	Al_2O_3	CaO	SiO_2	Al_2O_3	CaO	SiO_2	Al_2O_3	CaO
Chemical Composition	54.8	23.9	21.3	69.0	27.0	4.0	71.0	16.3	12.7
Quartz-free	44.0	29.7	26.3	55.5	38.7	5.7	43.8	31.6	24.7
Quartz-free and Simplified	36.7	24.7	38.6	41.5	28.6	29.9	34.1	24.6	41.3
Simplified	47.2	20.6	32.2	55.9	21.6	22.6	62.0	14.2	23.8

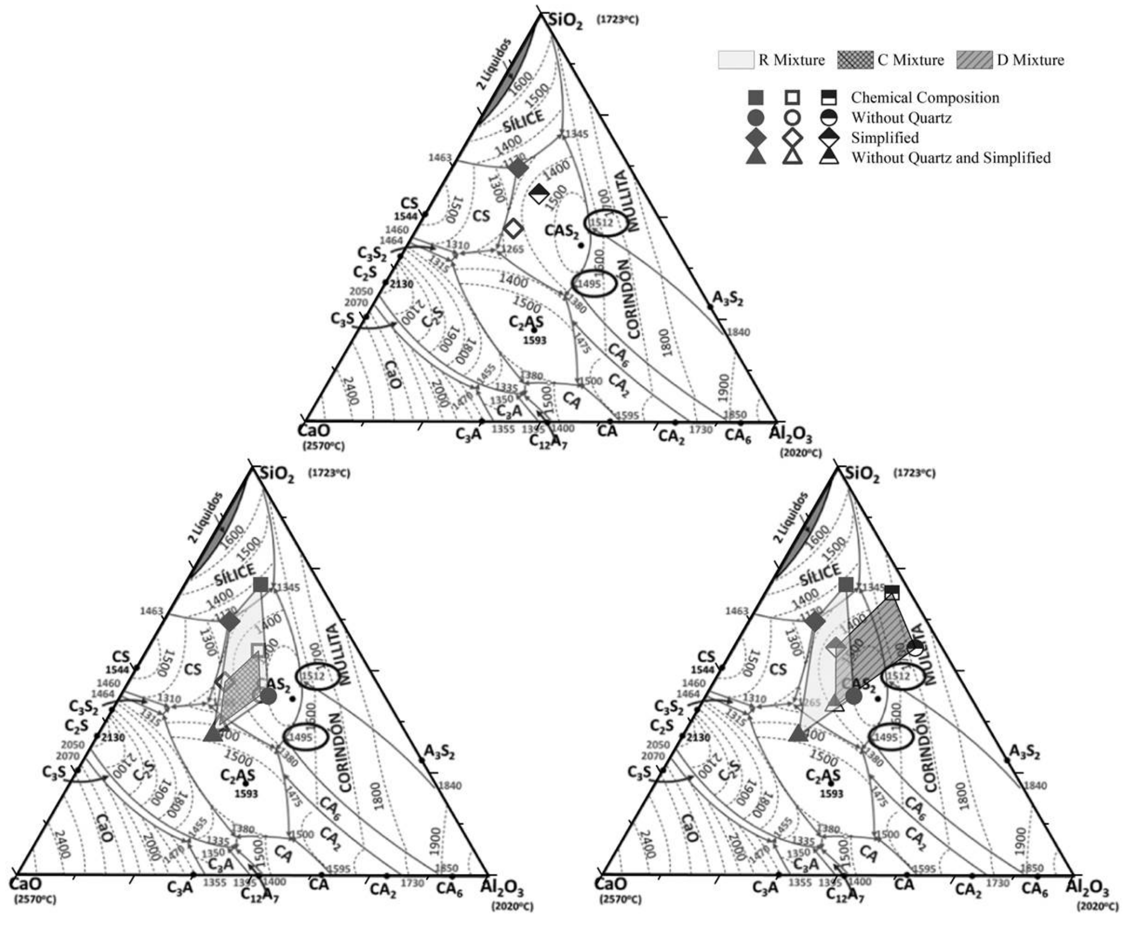

Figure 2: Representations of R, C and D materials in the SiO_2-Al_2O_3-CaO diagram

Additionally, the proposed waste-based materials formulations have also taken into consideration the waste mineralogical composition and they are expected to develop different sintering and technological behavior. In particular, material C formulation has aimed to optimize the proportion of SiO_2, Al_2O_3, and CaO so as to obtain a final ceramic material with abundant calcium crystalline phases such as anorthite, ghelenite and wollastinite (CAS_2, C_2AS and CS respectively, Figure 2, which may provide mechanical resistance and thermal insulation capacity at the expense of medium-high porosity. Thus, the chemical composition that most closely approximates the expected behavior is the simplified one, as it is located close to the eutectic point (1265ºC).

For its part, the mixture D formulation has intended to develop a material similar to C but with a lower content CaO, and a higher melting capacity, which would be provided by the greater amounts of amorphous SiO_2, Fe_2O_3, and K_2O (Table 1). As the CaO proportion decreases, the formulation region moves to the right of the ternary diagram towards the primary field of the mullite (Figure 2). This material is expected to be less porous than material C, so it would exhibit a higher mechanical strength and lower thermal insulation capacity. Again, the simplified chemical composition reflects the most this expected behavior.

3.2. Fired Materials Characterization

3.2.1. Mineralogical Characterization

From the mineralogical composition shown in Table 4, it can be said that material C has a greater quantity of crystalline phases than material D, such that, this is, therefore, the material with the highest volume of amorphous and/or non-diffracting material. This fact is in agreement with the formulation of the materials, as material C was designed to develop crystalline phases, while material D was designed to have a greater melting capacity and therefore a greater amount of vitro/amorphous material was developed. In this respect, it should be noted that the amorphous material present in the samples includes both the glass resulting from the formation of liquid at high temperature and the original crystalline phases that have lost crystallinity during heat treatment without reacting.

Table 4: Quantification (%) of the crystalline phases and vitreous/amorphous phases in the C and D materials at different sintering temperatures

	C Material			D Material		
	1000ºC	**1050ºC**	**1100ºC**	**1000ºC**	**1050ºC**	**1100ºC**
Quartz	7.0	6.8	4.3	13.0	12.9	12.9
Hematites	4.8	4.1	2.2	6.2	7.8	9.2
Sillimanite	-	-	-	2.9	3.0	2.9
Mullite	6.4	3.7	2.7	7.5	7.5	7.3
Diopside	-	-	-	2.5	2.3	2.0
Albite	-	-	-	6.0	9.0	10.9
Dolomite	-	-	-	1.3	1.5	1.6
Anortite	19.6	21.7	28.5	-	-	-
Gehlenite	11.3	11.5	11.5	-	-	-
Wollastonite	4.8	4.6	6.3	-	-	-
Akermanite	2.7	2.4	1.6	-	-	-
Magnesioferrite	0.5	1.0	1.3	-	-	-
Vitreous/Amorphous	42.8	44.2	41.6	60.5	56.1	53.2

If the evolution of the crystalline phases with the sintering temperature is analyzed, it is observed that there are no significant differences in the amount of gehlenite in material C, and of quartz, silimanite, mullite, dolomite and diopside in material D. The presence of undecomposed dolomite above 900 ºC may be feasible due to the conditions under which the thermal treatments were carried out. If during the heat treatment, the furnace atmosphere contains more than 25% CO_2, the carbonate decomposition reaction is inhibited [44]. This could be the case, since sintering was carried out at the same time and at the same temperatures for materials C and D, and both experience combustion of organic matter between 200 ºC and 850 ºC, as reflected in [15].

On the contrary, there are other phases that increase their content considerably in material C, such as anorthite, which rises from 19.6 wt% at 1000 ºC to 28.5 wt% at 1100 ºC, and wollastonite, whose proportion is 4.8 wt% at 1000ºC and 6.3 wt% at 1100 ºC. Hematite and albite experience a similar increase in material D, such that the former has a percentage of 6.2 wt% at 1000 ºC and 9.0 wt% at 1100ºC, while albite changes from 6.0 wt% at 1000 ºC to 10.9 wt% at 1100 ºC. By contrast, other phases, like quartz, hematite, akermanite and mullite are undermined, with reductions of 2.7 %, 2.6 %, 1.1 % and 3.7 % in material C, respectively when the temperature is increased from 1000 ºC to 1100 ºC. No significant disappearance of mineral phases is observed in material D.

However, not all quantified crystalline phases have been developed during thermal sintering treatments, since akermanite in material C, dolomite in material D and quartz, hematite and mullite in both materials, were originally present in the waste used as raw material [9]. The crystalline phases that have been developed in material C, are anortite, gehlenite, magnesioferrite and wollastonite, while in material D, are silimanite, diopside and albite. Both the anortite, the gehlenite and the wollastonite in the material C, as the diopside and the albite in the material D, are crystalline calcium phases, so the objective of obtaining these phases by mixing the residues and using the ternary diagram of phase equilibrium SiO_2-Al_2O_3-CaO has been achieved.

3.2.2. Microstructural Characterization

Figure 3 shows a series of micrographs corresponding to the sintered C material at 1000 ºC, 1050 ºC and 1100 ºC. These micrographs are characterized by a series of grains and/or particles embedded within the ceramic matrix. The porosity of these materials can be observed in the ceramic matrix, which is characterized for being open and highly interconnected at 1000 ºC, reducing the interconnection of the pores as the sintering temperature increases, without apparently varying in volume. The grains correspond to the crystalline phases present in the material (Table 4), whose origin is in the original waste used as raw material or their development during the heating treatments. In addition, microanalyses carried out on different grains show a chemical composition that coincides with the mineralogical phases determined by the Rietveld methodology. As the sintering temperature increases, the grain size decreases to become part of the glass phase or to form new crystalline structures of smaller size.

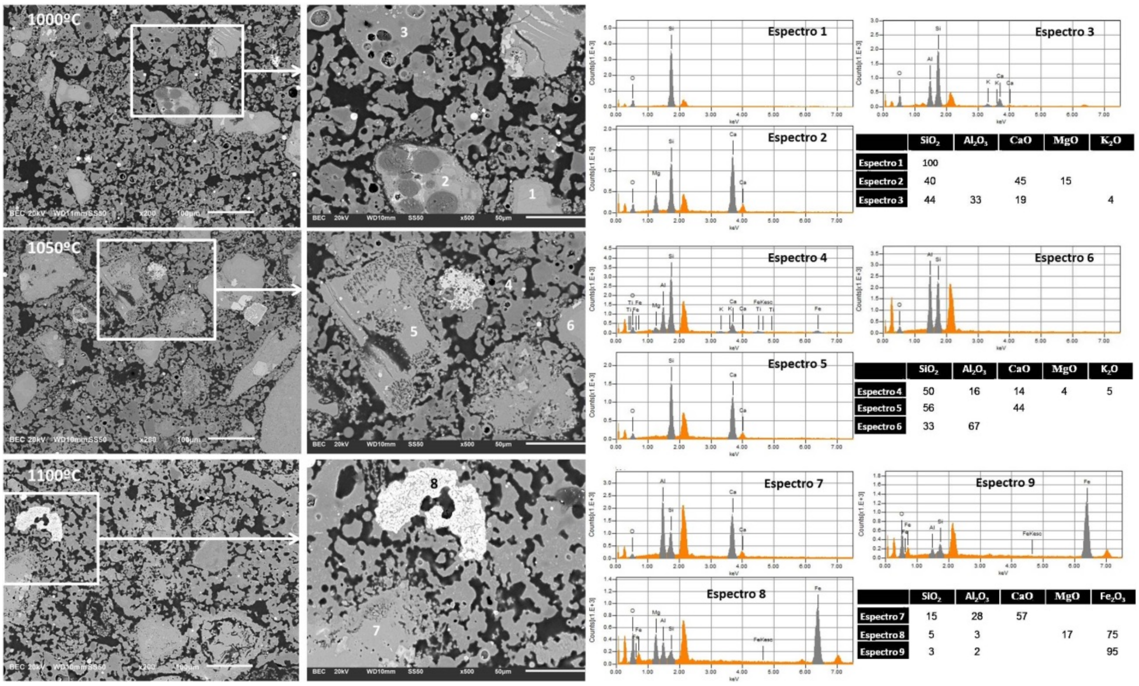

	SiO_2	Al_2O_3	CaO	MgO	K_2O
Espectro 1	100				
Espectro 2	40		45	15	
Espectro 3	44	33	19		4

	SiO_2	Al_2O_3	CaO	MgO	K_2O
Espectro 4	50	16	14	4	5
Espectro 5	56		44		
Espectro 6	33	67			

	SiO_2	Al_2O_3	CaO	MgO	Fe_2O_3
Espectro 7	15	28	57		
Espectro 8	5	3		17	75
Espectro 9	3	2			95

Figure 3: SEM micrographs of C material at three sintering temperatures. Left at x200 and right at x500 magnification and EDX microanalysis

Figure 4 shows a series of micrographs corresponding to material D sintered at 1000 °C, 1050 °C and 1100 °C. The grains present in the microstructure of material D are totally different from those of material C, such that the former have grains that are much more rounded and smaller than those from material C. In addition, there is a granular structure with a high internal porosity and many spherical white bodies, which may be attributed to the oil diatomaceous earths and the hematite of fly ash respectively, both used as raw materials for the manufacture of this material. In the ceramic matrix (Figure 4), the porosity of these materials can be observed, characterized by a certain amount of closed porosity and a higher amount of open and interconnected porosity at 1000 ºC, which decreases significantly as the sintering temperature increases and the internal porosity of the grains that originate in diatomaceous earth remains stable. The microanalyses performed on the grains present in material D (Figure 4) are in accordance with the mineralogical phases developed (Table 4).

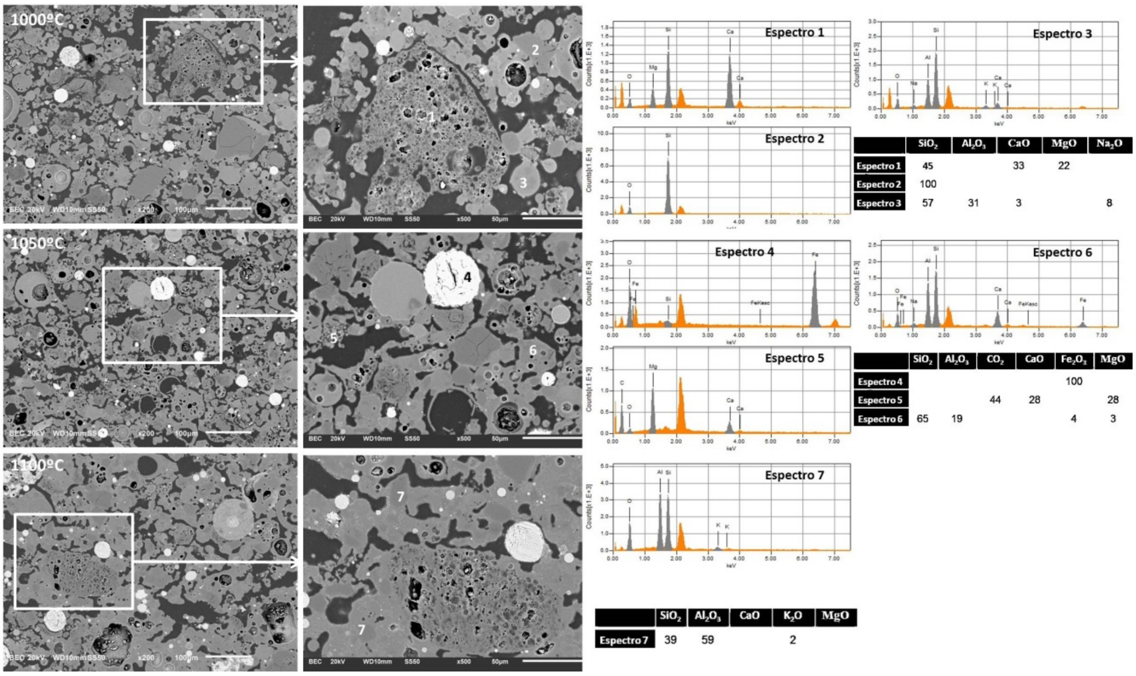

	SiO_2	Al_2O_3	CaO	MgO	Na_2O
Espectro 1	45		33	22	
Espectro 2	100				
Espectro 3	57	31	3		8

	SiO_2	Al_2O_3	CO_2	CaO	Fe_2O_3	MgO
Espectro 4					100	
Espectro 5			44	28		28
Espectro 6	65	19			4	3

	SiO_2	Al_2O_3	CaO	K_2O	MgO
Espectro 7	39	59		2	

Figure 4: SEM micrographs of D material at three sintering temperatures. Left at x200 and right at x500 magnification and EDX microanalysis

Figure 5 shows the distribution and pore size graphs of the materials C and D sintered at 1000 ºC, 1050 ºC and 1100 ºC. As can be seen in the graphs, both materials have a bimodal pore distribution, i.e. they have two different pore sizes embracing between 80 % and 90 % of the porosity, regardless of the sintering temperature. In material C, the predominant pore sizes are ~3 µm and ~6.5 µm, while in material D they are ~4 µm and ~7 µm. In addition, although the amplitude of the joint distribution is greater in material C than in D, the distribution peaks are more intense in material D than in C, which implies a greater amount of pore with the same size. The remaining porosity is divided into a porosity with a pore size greater than 15 µm, being this porosity similar in both materials, and a porosity with a pore size smaller than 0.5 µm. In this porosity range, material C has a much smaller number of pores than material D, Table 5.

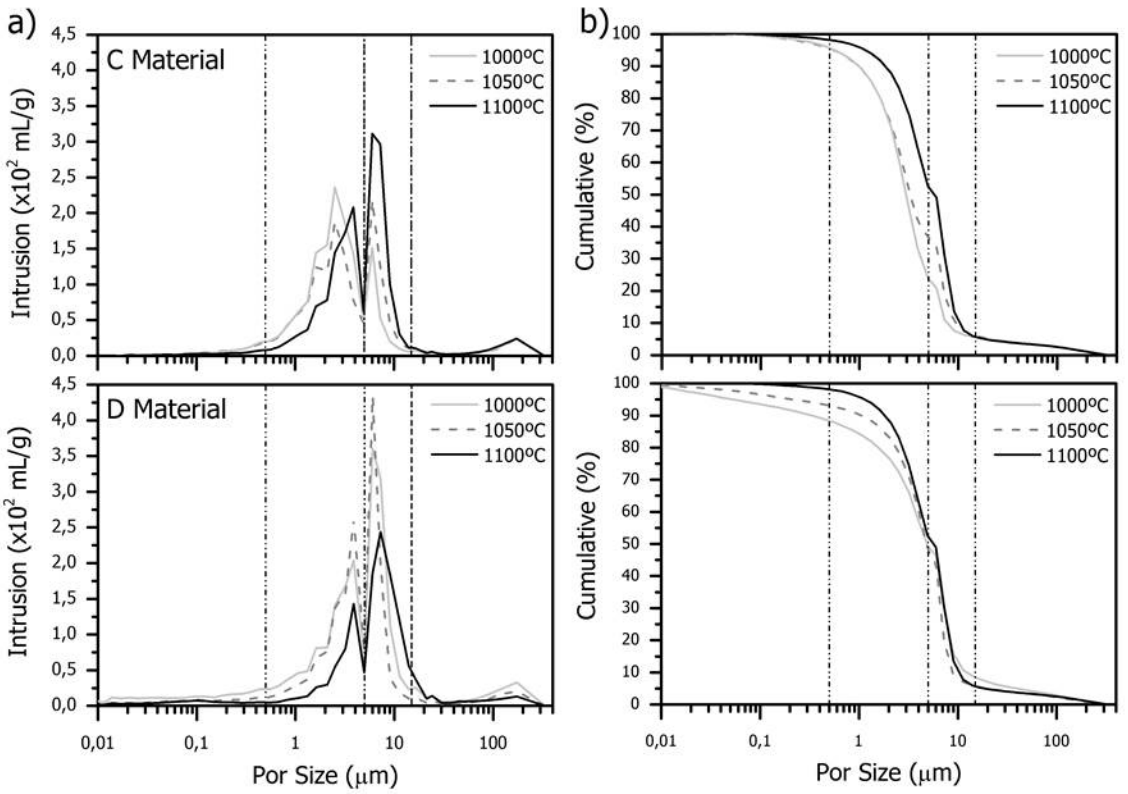

Figure 5: Pore size distribution of C and D material at three sintering temperatures. a) Intrusion and b) cumulative

Table 5: Porosity intervals, Main Pore Size and Open Porosity of C and D materials at three sintering temperatures

Porosity Intervals	**C Material**						**D Material**					
	1000ºC		**1050ºC**		**1100ºC**		**1000ºC**		**1050ºC**		**1100ºC**	
	%	**T***	**%**	**T***	**%**	**T***	**%**	**T***	**%**	**T***	**%**	**T***
< 0.5 µm	5	-	5	-	2	-	12	-	7	-	2	-
0.5 < x < 5 µm	72	2.5	59	2.5	46	3.8	40	3.9	46	3.9	46	3.8
5 < x < 15 µm	18	6.0	31	6.1	47	6.9	40	6.3	42	6.2	47	7.3
> 15 µm	5	-	5	-	5	-	8	-	5	-	5	-
Open Porosity (%)	28.7		29.3		30.3		34.5		30.0		26.4	

T*: Pore size that has the highest intrusion volume, being the pore size more repeated

When the sintering temperature increases from 1000 ºC to 1100 ºC, those pores below 0.5 μm disappear due to the formation of the liquid phase that fills the pores . This process takes place on a larger scale in material D due to its greater melting capacity, going from a 12 % of pores less than 0.5 μm at 1000 ºC to 2 % at 1100 ºC in material D and from 5 % to 2 % when the temperature is increased to 1100 ºC in material C. However, the porosity above 15 μm remains constant in both materials when the sintering temperature is modified (Table 5).

In the porosity range between 0.5 μm and 5 μm, the behavior of both materials with the sintering temperature is the opposite. In material C, porosity in this pore size range decreases with increasing sintering temperature from 72 % at 1000 °C to 46 % at 1100 °C, resulting in an increase in pore size from 2.5 μm to 3.8 μm. However, in material D, there is an increase in porosity with the sintering temperature, from 40 % to 46 % as the temperature rises from 1000 °C to 1050 °C, maintaining a constant pore size of ~3.9 μm (Table 5).

In the porosity range between 5 μm and 15 μm, material D behaves in the same way as the previous range, except that its pore size increases from 6.3 μm to 7.3 μm as the temperature increases from 1000 °C to 1100 °C. However, in material C there is a significant increase in porosity in this range of pore-size, from 18 % at 1000 ºC to 47 % at 1100 ºC, accompanied by an increase in pore size, Table 5.

The porosity behaviour reflected in material C is characteristic of ceramic materials with crystalline calcium phases formation, as these produce an increase in pore size without a significant variation in total pore volume [43]. This is in accordance with the crystalline calcium phases developed in this material, such as wollastonite, gehlenite and anorthite, as shown by the mineralogical composition developed by the sintered C material (Table 4).

In addition to the pore size and distribution, the mercury intrusion porosimetry allows to determine the open porosity of the analyzed materials. Table 5 shows the open porosity values of sintered C and D materials at 1000 °C, 1050 °C and 1100 °C. According to these data, material C has a practically constant porosity when the sintering temperature is varied, with a minimum value of 28.7 % at 1000 ºC and a maximum value of 30.3 % at 1100 ºC, in accordance with the microstructure shown in Figure 3. However, material D experiences a decrease in its open porosity values, which is directly proportional to the increase in sintering temperature, from a value of 34.5 % at 1000 ºC to 26.4% at 1100ºC, which is characteristic of materials with high melting capacity (Figure 4).

3.3. Technological Properties

The results obtained from the technological characterization of the sintered materials are shown in Table 6.

Table 6: Technological properties of C and D materials at three sintering temperatures

		Density (g/cm^3)	**Water Absorption (%)**	**Bending Strenght (kg/cm^2)**	**Thermal Conductivity (W/mK)**
C	**1000ºC**	1.87 ± 0.01	17.8 ± 0.1	85 ± 3	0.67 ± 0.02
	1050ºC	1.85 ± 0.01	18.9 ± 0.3	96 ± 8	0.68 ± 0.02
	1100ºC	1.83 ± 0.01	19.6 ± 0.4	159 ± 10	0.70 ± 0.02
D	**1000ºC**	1.57 ± 0.01	24.2 ± 0.3	74 ± 5	0.40 ± 0.02
	1050ºC	1.69 ± 0.01	20.1 ± 0.1	131 ± 3	0.51 ± 0.03
	1100ºC	1.86 ± 0.01	15.1 ± 0.3	147 ± 7	0.63 ± 0.03

As can be observed in Table 6, the apparent density value decreases with increasing the temperature from 1.87 g/cm^3 at 1000 ºC to 1.83 g/cm^3 at 1100 ºC in material C, while it increases from 1.57 g/cm^3 to 1000 ºC to 1.86 g/cm^3 to 1100 ºC in material D, so the variation in density of material C is significantly less than that shown in material D, being these variations of 2.1 % and 18.5 % for materials C and D respectively with respect to the density value at 1000 ºC.

The behavior shown in material C is characteristic of refractory materials which maintain a dimensional stability with temperature variations without modifying their dimensions [45] and their density. On the other hand, the significant variation in density with the sintering temperature shown in material D is due to its high melting capacity, which causes a significant contraction or reduction in volume when the temperature increases from 1000 ºC to 1100 ºC, with values of 1.57 g/cm^3 and 1.86 g/cm^3, respectively.

In addition, the density variations in both materials with sintering temperature are opposite, since while the density of material C decreases with higher temperatures, the density of material D increases. These density variations are directly proportional to the porosity differences (Table 6) that materials experience with the temperature, since an enhancement of the porosity of material C from 2.1 % to 3.5 % when the temperature increases from 1050 ºC to 1100 ºC, respectively, corresponds to a decrease in the density of 1.0 % and 1.1 %, respectively. Conversely, for material D, a decrease in porosity of 13.1 % and 12.0 % results in an increase in density of 7.7 % and 10.1 %, respectively.

Furthermore, the water absorption values show the opposite trend to apparent density, as the value of the water absorption capacity increases with the sintering temperature from 17.8 % at 1000°C to 19.6 % at 1100 °C in material C, while it drops from 24.2 % at 1000 °C to 15.1 % at 1100 °C in material D, so that the variation in the water absorption of material C is significantly less than that shown by material D. The behavior of this technological parameter is directly related to the porosity of the materials, so that if the development of material C is fostered with the sintering temperature (Table 5), there is an associated increase in the water absorption capacity. Similarly, a decrease in the porosity of material D results in a reduction of the water absorption.

However, the mechanical resistance is improved with the sintering temperature, since it changes from 85 kg/cm^2 and 74 kg/cm^2 at 1000 ºC to 159 kg/cm^2 and 147 kg/cm^2 at 1100 ºC for materials C and D, respectively (similar behavior in both materials). Nonetheless, this effect is opposite to the apparent density evolution of material C, because while the increase in density in material D increases its resistance, while the enhancement of mechanical strength is linked to lower density values in material C. This is due to the fact that the increase in resistance in material D is associated with the decrease in porosity produced by the formation of the molten phase that fills the pores and increases the density of the material. However, in material C, as there is no decrease in porosity, the increase in resistance is caused by the formation, during heat treatment, of crystalline phases, such as anorthite, whose concentration raised 10.7 % at 1050 ºC with respect to its value at 1000 ºC and 31.3 % at 1100 ºC with respect to 1050 ºC. These crystalline phases' gain is associated with an increase of the mechanical strength of 12.9 % at 1050 ºC and 65.6 % at 1100 ºC.

As shown in the Thermal Conductivity data shown in Table 6, the conductivity values grow with the sintering temperature from 0.67 W/mK and 0.40 W/mK at 1000°C to 0.70 W/mK and 0.63 W/mK at 1100 °C for materials C and D, respectively. The behavior described by this property in material D is logical, since as the material densifies with the sintering temperature and the thermal conductivity, its porosity diminishes (Table 5). This is due to the fact that by decreasing the porosity, the continuity of the solid phase of the material increases, as shown by the microstructures in Figure 4, favoring the mechanisms of heat transmission by conduction. However, in material C, as the sintering temperature turns higher, the thermal conductivity is also augmented, as happened with material D (Table 6), albeit its apparent density values decrease and the open porosity ones increase. However, these variations in the values of apparent density, open porosity and thermal conductivity in material C are very small and it could be considered almost constant.

Anyway, to explain this behavior of the thermal conductivity with respect to the sintering temperature in material C, it is necessary to use other factors, since porosity alone does not explain it. It could be related to the refractory nature of this material and the structural modifications that the material undergoes as the crystalline calcium phases are developed. Figure 6 shows the linear relationship between the open porosity of the sintered materials and their thermal conductivity values.

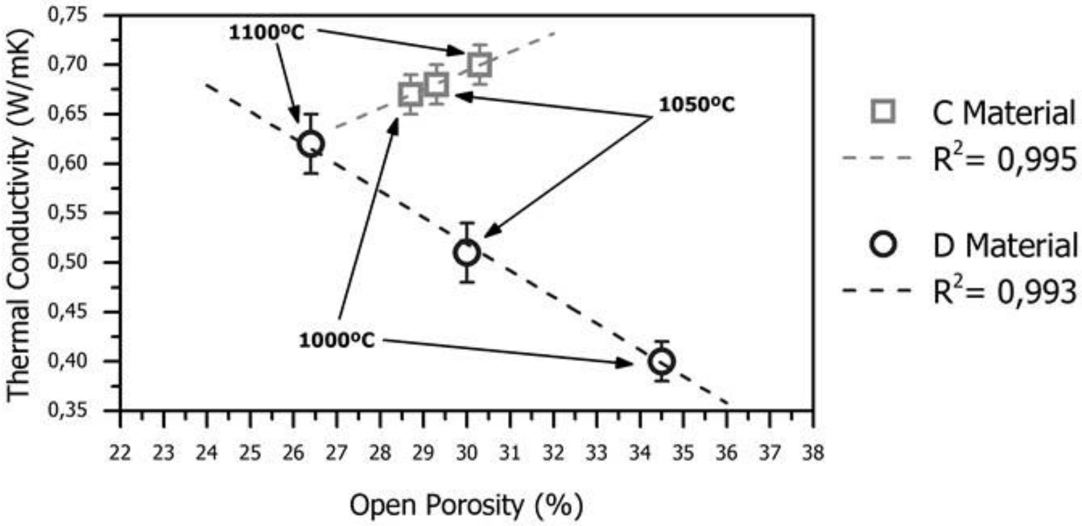

Figure 6: Relationship between thermal conductivity and open porosity

Besides that, the open porosity increases with the development of the crystalline calcium phases, as shown by the data shown in Table 5, resulting in an increase in size from 2.5 µm to 3.8 µm and from 6.0 µm to 6.9 µm in the porosity ranges between 0.5 µm-5 µm and 5 µm-15 µm for sintering temperatures of 1000 ºC and 1100 ºC, respectively. This causes the pore specific surface to decrease and the continuity of the solid phase to increase, as shown by the microstructure of material C (Figure 3). If we add to this fact an increase in the skeletal density of the materials (Table 7), considered as the density of the solid fraction of the material, it can be understood that the thermal conductivity of material C becomes higher when the sintering temperature increases.

Table 7: Skeletal density values obtained by helium picnometry

	C Material			**D Material**		
	1000ºC	**1050ºC**	**1100ºC**	**1000ºC**	**1050ºC**	**1100ºC**
Skeletal Density (g/cm^3)	2.862	2.881	2.897	2.745	2.746	2.742

4. Conclusions

The industrial waste used in this work, electric arc furnace stainless steel ashes, fly and bottom ash from coal power plants, and diatomaceous earth from the filtration of industrial oils can be used as raw materials for obtaining ceramic materials. This fact would reduce the environmental impact generated by the industrial sectors that produce these wastes and, in addition, it would be possible their valorization into raw materials for other production processes, like the manufacture of ceramic materials, thus reducing the consumption of natural resources.

The original idea of formulating ceramic building materials by the use of resides as a raw material is feasible, since a correct consolidation and sinterization is achieved by different mechanisms as has been demonstrated in this work, either by the formation of crystalline phases, like in material C, or by the appearance of liquid phase (melting capacity) during the thermal treatments.

In addition, the use of ternary equilibrium diagrams, a common formulation tool applied to conventional ceramics, is useful to design formulations of waste-based ceramic materials, since it is possible to arrange the most suitable compositions to the needs required according to the chemical composition and the target materials to be obtained, controlling the mineralogy of the raw materials.

Thus, the design of the formulation of material C to develop calcium crystalline phases is significantly achieved by placing it within the primary field of the anorthite in the ternary equilibrium SiO_2-Al_2O_3-CaO diagram, since the crystalline phases developed during the heat treatment, such as anortite, gehlenite or wollastonite, represent 63.3 wt%, 69.5 wt% and 81.5 wt% of the total ones present in the material C when sintered at 1000 ºC, 1050 ºC and 1100 ºC, respectively. Moreover, in material D, there are not many crystalline phases developed during the thermal treatment, representing only 28.8%, 32.5% and 33.7 % at the abovementioned sintering temperatures, 1000 ºC, 1050 ºC and 1100 ºC, respectively, because of their reduced Ca content and the higher presence of amorphous silica. The main develop phases are silimanite, diopside and albite.

All materials manufactured from both compositions at different sintering temperatures are technically viable materials, since the final properties obtained have suitable values for use as building materials, with the exception of material D sintered at 1000 ºC, which has an acceptable bending strength but a high water absorption capacity value, according to its low bulk density. Depending on the technological properties, the optimum sintering temperature for both material C and D is 1100 ºC, temperature at which the highest bending mechanical strength results were obtained along with appropriate values of apparent density, water absorption capacity and thermal conductivity.

Acknowledgement

This work was funded by the SMARTMATS Project, (MAT2015-70034-R, Spanish Ministry of Economy and Competitiveness). Technical and human support provided by CICT of Universidad de Jaén (UJA, MINECO, Junta de Andalucía, FEDER) is gratefully acknowledged. Support from the EFIWALL Project (PI12/1920, Junta de Andalucía) is also acknowledged.

References

[1] Environmental management systems - Guidelines for incorporating ecodesign (ISO 14006:2011)

[2] https://ec.europa.eu/programmes/horizon2020/en/h2020-section/climate-action-environment-resource-efficiency-and-raw-materials.

[3] Barbieri, L., Andreola, F., Lancellotti, I., Taurino, R. Management of agricultural biomass wastes: preliminary study on characterization and valorisation in clay matrix bricks. Waste Manag. 11, 2307–2315 (2013)

[4] Demir, I. Effect of organic residues addition on the technological properties of clay bricks. Waste Manag. 28, 622–627 (2008)

[5] Raut, S.P., Ralegaonklar, R.V., Mandavgane, S.A. Development of sustainable construction material using industrial and agricultural solid waste: a review of waste-create bricks. Constr. Build. Mater. 25, 4037–4042 (2011)

[6] Zhang, L. Production of brick from waste materials – A Review. Construction and Building Materials. 47, 643-655 (2013)

[7] De Aza, A, H., Pena, P., Caballero, A., Dd Aza, S. The phase equilibrium diagrams as a tool for the design and use of refractories. Boletín de la Sociedad Española de Ceramica y Vidrio, 50 (6) 279-290 (2011)

[8] Fiori, C., Fabbri, B., Donati, F., Venturi, I.. Mineralogical composition of the clay bodies used in the Italian tile industry. Appl. Clay Sci. 4 (5-6) 461-473 (1989). http://dx.doi.org/10.1016/0169-1317(89)90023-9

[9] González, I., Galán, E., Miras, A., Aparicio, P. New uses for brick-making clay materials from the Bailén area (southern Spain). Clay Minerals, 33 (3) 453-465 (1998)

[10] El-Mahhllwy, M. S. Characteristics of acid resisteng bricks made from quarry residues and waste steel slag. Construction and Building Materials, 22, 1887-1896 (2008)

[11] Galán-Arboledas, R. J., Álvarez de Diego, J., Dondi, M. Bueno, S. Energetic, Environmental and Technical Assessment for the Incorporation of Waste Steel Slag in Ceramic Building Materials. Journal of Cleaner Production, 142, 1778-1788 (2017)

[12] Kavouras, P. et al. Glass-ceramic materials from electric arc furnace dust. Journal of Hazardous Materials, 139, 424-429 (2007)

[13] Pai-Haung Shih, Zong-Zheng Wu, Hung-Lung Chiang. Characteristics of bricks made from waste steel slag. Waste Management, 24, 1043–1047 (2004)

[14] Feng He, Yu Fang, Junlin Xie, Jun Xie. Fabrication and characterization of glass–ceramics materials developed from steel slag waste. Materials and Design, 42, 198–203 (2012)

[15] Galán-Arboledas, R. J., Bueno, S. Production of ceramic materials using only waste as raw materials. Key Engineering Materials, 663, 62-71 (2016)

[16] Ponsot, I., Bernardo, E. Self-glazed glass ceramic foams from metallurgical slag and recycled glass. Journal of Cleaner Production, 59, 245-250 (2013)

[17] Yu-Ling Weia et al. Recycling steel-manufacturing slag and harbor sediment intoconstruction materials. Journal of Hazardous Materials, 265, 253–260 (2013)

[18] Favoni, C. et al. Ceramic processing of municipal sewage sludge (MSS) and steelworks slags (SS). Ceramics International, 31, 697–702 (2005)

[19] Baruzzo, D. et al. Possible production of ceramic tiles from marine dredging spoils alone and mixed with other waste materials. Journal of Hazardous Materials, B-134, 202–210 (2006)

[20] Lihua Zhao, Yu Li, Yuanyuan Zhou, Daqiang Cang. Preparation of novel ceramics with high CaO content from steel slag. Materials and Design, 64, 608–613 (2014)

[21] Chen, Y. et al. Preparation of eco-friendly construction bricks from hematite tailings. Constructions and Building Materials, 25, 2107–2111 (2011)

[22] Lingling, X., Wei, G. Tao W, Nanru Y. Study on fired bricks with replacing clay by fly ash in high volume ratio. Constructions and Building Materials, 9, 243–247 (2005)

[23] Romero, M., Rincón, J. M. The controlled vitrification/crystallisation process applied to the recycling of inorganic industrial wastes. Boletín de la Sociedad Española de Cerámica y Vidrio, 39 (1) 155-163 (2000)

[24] Aineto, M., Acosta, A., Rincón, J. M., Romero, M. The slag from ELCOGAS IGCC thermal power plant as raw material for the synthesis of glass-ceramic materials. Part 2: Synthesis and characterization of the glass-ceramic materials. Boletín de la Sociedad Española de Cerámica y Vidrio, 45 (1), 28-32 (2006)

[25] Kockal, N. U. Utilisation of different types of coal fly ash in the production of ceramic tiles. Boletín de la Sociedad Española de Cerámica y Vidrio, 51(5), 297-304 (2012)

[26] Alaa A. Shakir, Naganathan, S., Nasharuddin, K., Mustapha. Properties of bricks made using fly ash, quarry dust and billet scale. Construction and Building Materials, 41, 131-138 (2013)

[27] Vinai, R., Lawane, A., Minane, J. R., Amadou, A. Coal combustion residues valorisation: Research and development on compressed brick production. Construction and Building Materials, 40, 1088-1096 (2013)

[28] Andreola, F., Barbieri, L., Lancellotti, I., Pozzi, P. Recycling industrial waste in brick manufacturing. Part 1. Mater. Construcc., 55 (280), 5-16 (2005)

[29] Kute, S., Deodhar, S.V. Effect of fly ash and temperature on properties of burnt clay bricks. Journal of Civil Engineering, 84, 82–85 (2003)

[30] Chou M., Patel, V., Laird, C.J., Ho, K.K. Chemical and engineering properties of fired bricks containing 50 weight per cent of class F fly ash. Energy Sources, 23, 665–673 (2001)

[31] Queralt, I., Querol, X., Lopez-Soler, A., Plana, F. Use of coal fly ash for ceramics. Fuel, 76 (8), 787-791 (1997)

[32] Ahmaruzzaman, M. A review on the utilization of fly ash. Program Energy Combustion, 36, 327-363 (2010)

[33] Menendez, E. et al. Characterization of bottom ashes from coal pulverized power plants to determine their potential use feasibility. Boletín de la Sociedad Española de Ceramica y Vidrio, 52 (6), 296-304 (2013)

[34] Monteiro, S.N., Vieira, C.M.F. Effect of oily waste addition to clay ceramic. Ceramics International, 31 (2), 353-358 (2005)

[35] Eliche-Quesada, D. et al. Recycling of sawdust, spent earth from oil filtration, compost and marble residues for brick manufacturing. Constructions and Building Materials, 34, 275–284 (2012)

[36] Hadjar, H. et al. Elaboration and characterization of new mesoporous materials from diatomite and charcoal. Microporous Mesoporous Materials, 107, 219–226 (2007)

[37] Lin, K.L., Lan, J.Y. Water Retention Characteristics of Porous Ceramics Produced from Waste Diatomite and Coal Fly Ash. Journal of Clean Energy Technologies, 1 (3), 211-215 (2013)

[38] Mymrine, V. et al. Oily diatomite and galvanic wastes as raw materials for red ceramics fabrication. Constructions and Building Materials, 41, 360–364 (2013)

[39] Gencel, O. et al. Properties of bricks with waste ferrochromium slag and zeolite. Journal of Cleaner Productions, 59, 111-119 (2013)

[40] Galán-Arboledas, R. J., Cotes, T., Martínez, C., Bueno, S. Influence of waste addition on the porosity of clay based ceramic membranes. Desalination and Water Treatment, 2633-2639 (2015) http://dx.doi.org/10.1080/19443994.2015.1017011.

[41] Zhenzi J., Hirotaka, M., Ioku, K., Ishida, E. Hydrothermal synthesis of mesoporous materials from diatomaceous earth. Materials, Interfaces and Electrochemical Phenomena, 53 (8), 2114-2122 (2007)

[42] Galán-Arboledas, R.J., Merino, A., Bueno, S. Use of new raw materials and industrial wastes to improve the possibilities of using ceramic materials from Bailén (Jaén, southern Spain). Mater. Construcc, 63 (312), 553-568 (2013).

[43] Serra, M.F., Acebedo, M.F., Conconi, M.S., Suarez, G., Aglietti, E.F., Rendtorff, N.M. Thermal evolution of the mechanical properties of calcareous earthware. Ceramics International, 40, 1709-1716 (2014).

[44] Galán-Arboledas, R. J. End of Master Project: Development of a new hydraulic binder from marl from the Province of Jaén. University of Jaén. October, 2014.

[45] Fabbri, B., Dondi, M. Caratteristiche e difetti del laterizio. Gruppo Editoriale Faenza Editrice S.p.A. Faenza (1995)